

Wavelet neural network modeling in QSPR for prediction of solubility of 25 anthraquinone dyes at different temperatures and pressures in supercritical carbon dioxide

R. Tabaraki, T. Khayamian*, A.A. Ensafi

Department of Chemistry, Isfahan University of Technology, Isfahan 84154, Iran

Received 29 October 2005; received in revised form 31 October 2005; accepted 31 October 2005

Available online 5 December 2005

Abstract

A wavelet neural network (WNN) model in quantitative structure property relationship (QSPR) was developed for predicting solubility of 25 anthraquinone dyes in supercritical carbon dioxide over a wide range of pressures (70–770 bar) and temperatures (291–423 K). A large number of descriptors were calculated with Dragon software and a subset of calculated descriptors was selected from 18 classes of Dragon descriptors with a stepwise multiple linear regression (MLR) as a feature selection technique. Six calculated and two experimental descriptors, pressure and temperature, were selected as the most feasible descriptors. The selected descriptors were used as input nodes in a wavelet neural network (WNN) model. The wavelet neural network architecture and its parameters were optimized simultaneously. The data was randomly divided to the training, prediction and validation sets. The predictive ability of the model was evaluated using validation data set. The root mean squares error (RMSE) and mean absolute errors were 0.339 and 0.221, respectively, for the validation data set. The performance of the WNN model was also compared with artificial neural network (ANN) model and the results showed the superiority of the WNN over ANN model.

© 2005 Elsevier Inc. All rights reserved.

Keywords: Anthraquinone dyes; Supercritical carbon dioxide; WNN

1. Introduction

Supercritical carbon dioxide (SC-CO₂) has been used as a solvent in dyeing of textiles and fibers [1–4]. This technique has several advantages relative to conventional wet process such as complete separation of the remaining dyestuff from the solvent, no use of surfactants, dispersing agent and drying process, save energy consumption (roughly up to 50%) and reduction of the amount of the waste water [5]. However, in order to apply supercritical fluid dyeing (SFD), it is necessary to be familiar with the solubility of dyes in SC-CO₂. This information is required to select a suitable dye and to optimize dyeing process. The anthraquinone and azo dyes have been used more than others in the SFD process. The solubility measurements of the anthraquinone dyes in supercritical carbon dioxide have been reported in terms of mole fraction of solute in solution in several papers [6–22]. These experimental data are correlated by theoretical or semi-empirical models [23–32]. In addition to

those hard modeling methods, some software methods such as artificial neural network (ANN) [33] have also been used for the prediction of solubility in supercritical conditions. Recently we have used wavelet neural network (WNN) for the prediction of the solubility of some polycyclic aromatic hydrocarbons in SC-CO₂ [34].

In this work, stepwise MLR was used to select the most informative descriptors from the calculated descriptors by Dragon software. The selected descriptors were used to develop a WNN model for predicting the solubility for 25 anthraquinone dyes in supercritical carbon dioxide over a wide range of pressures (70–770 bar) and temperatures (291–423 K).

2. Theory

2.1. Wavelet

Wavelet transform (WT) is a novel signal processing technique developed from the Fourier transform and has been widely used to signal processing. The main characteristic of wavelet transform is its time-frequency localization. Wavelet

* Corresponding author. Tel.: +98 311 391 2351; fax: +98 311 391 2350.
E-mail address: taghi@cc.iut.ac.ir (T. Khayamian).

transformation (WT) has versatile basis functions to be selected based on the type of the signal analyzed. In WT, all basis function $\psi_{a,b}(x)$ can be derived from a mother wavelet $\psi(x)$ through the following dilation and translation processes:

$$\psi_{a,b}(x) = a^{-1/2} \psi\left(\frac{x-b}{a}\right), \quad a, b \in R \text{ and } a > 0 \quad (1)$$

where the parameters of translation are $b \in R$ and of dilation are $a \in R$ and $a > 0$ (R denotes real number). The mother wavelet, $\psi(x)$, is a single fixed function such as Morlet function from which, all basis functions are generated.

The applications of wavelet in chemistry have been reviewed in several papers [35] and books [36,37].

2.2. Wavelet neural networks

Wavelet neural network (WNN) is an approach towards the learning function. Wavelet networks, which combine the wavelet theory and feed-forward neural networks, utilize wavelets as the basis function to construct a network. Wavelet function is a local function and influence the networks output only in some local range. The wavelet neural network shows surprising effectiveness in solving the conventional problems of poor convergence or even divergence encountered in other kinds of neural networks. Guo et al. have used WNN for prediction of driving forces of α -cyclodextrin complexation with benzene derivatives and the inclusion of β -cyclodextrin with benzene derivatives [38,39]. Zhang et al. have been used WNN for prediction of programmed temperature retention values of naphthas [40].

The topological structure of the WNN employed in this study is shown in Fig. 1. The WNN consists of three layers: input layer, hidden layer and output layer. The detailed description of the calculation steps of WNN are explained in Ref. [41]. In brief, the connections between input units and hidden units are called weights u_{ji} and between hidden units and output units are called w_i . A Morlet mother function is used as node activation function for the hidden layer. The dilation and translation parameters, a_i and b_i , of the Morlet function for each node in the hidden layer are different. These parameters including w_i , u_{ji} , a_i , b_i are adjusted by the gradient descend

algorithm for obtaining the minimum error function (E). These parameters are adjusted using:

$$\Delta w_i^{\text{new}} = -\eta \frac{\partial E}{\partial w_i^{\text{old}}} + \alpha \Delta w_i^{\text{old}} \quad (2)$$

$$\Delta u_{ji}^{\text{new}} = -\eta \frac{\partial E}{\partial u_{ji}^{\text{old}}} + \alpha \Delta u_{ji}^{\text{old}} \quad (3)$$

$$\Delta a_i^{\text{new}} = -\eta \frac{\partial E}{\partial a_i^{\text{old}}} + \alpha \Delta a_i^{\text{old}} \quad (4)$$

$$\Delta b_i^{\text{new}} = -\eta \frac{\partial E}{\partial b_i^{\text{old}}} + \alpha \Delta b_i^{\text{old}} \quad (5)$$

The error function E is taken as

$$E = \frac{1}{2} \sum_{n=1}^N (v_n^T - v_n)^2 \quad (6)$$

where v_n^T and v_n are the experimental and calculated values, respectively. N stands for the data number of training set, and η and α being the learning rate and the momentum term, respectively. The iteration process is continued until the network output meets the error criteria.

3. Data and methodology

3.1. Data set

The data set consists of 25 anthraquinone dyes that their structures are given in Table 1. The experimental values of solubility at different temperature and pressure were collected from the following references: (Blue 14, Orange 11 and 1-methylaminoanthraquinone) [6]; (Red 11 [7]; (Red 60 and Blue 60) [8]; Blue 3 [10]; Blue 134 [11]; (Blue 27, Blue 77 and Blue 118) [12]; (AQ1, AQ2, AQ3, AQ4, AQ5, AQ6, AQ7) [14]; (A1, A2, A3, A4) [15]; Quinizarin [16]; ACO3 [20] and ACO8 [21]. The data set consists of 760 experimental values of the solubility for 25 anthraquinone dyes in different temperatures and pressures. The data set of 15 anthraquinone dyes was randomly divided into two data sets: training (249) and prediction (121) data sets. The remaining data were employed for the validation data set. The validation data set (390 data) consists of two data sets, in which the differences in the sets are related to the types of the molecules. The first data set consists of the molecules with the same molecular structures as those of the molecules in the training and prediction set. The second data set comprises of ten anthraquinone molecules, with molecular structures which are new for the model. The molecular structures of those molecules are given in Table 1 (the last 10 molecules).

3.2. Descriptor calculation

All molecules were drawn in the HyperChem 6 [42] software. The optimization of the molecular structures was also carried out by semi-empirical AM1 method using the Fletcher–Reeves algorithm until the root mean square gradient was 0.01.

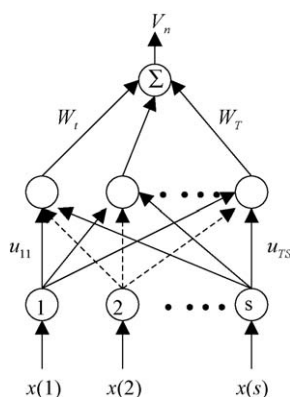


Fig. 1. The WNN topology structure.

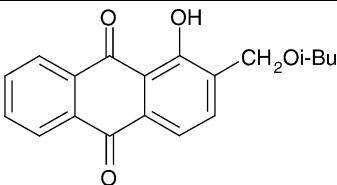
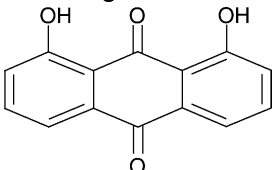
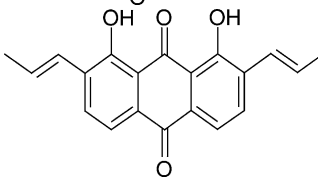
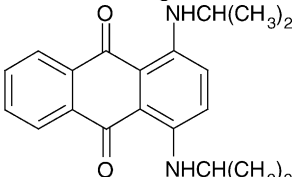
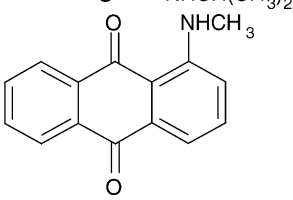
Table 1
Molecular structure of anthraquinone dyes

Dyes	Molecular structure
1 Blue 14	
2 Red 11	
3 Red 60	
4 Blue 60	
5 Blue 27	
6 Blue 118	
7 AQ1	
8 AQ3	
9 AQ5	
10 AQ6	

Table 1 (Continued)

Dyes	Molecular structure
11 A2	
12 A3	
13 ACO3	
14 ACO8	
15 Quinizarin	
16 Orange 11	
17 Blue 3	
18 Blue 77	
19 AQ2	
20 AQ4	

Table 1 (Continued)

	Dyes	Molecular structure
21	AQ7	
22	A1	
23	A4	
24	Blue 134	
25	1-Methyl aminoanthraquinone	

The resulted geometry was loaded into Dragon software [43] to calculate 1481 descriptor in 18 different classes. All computations were carried out on a Pentium 4, 1.5 GHz PC computer. Multiple linear regression analysis of molecular descriptors and logarithm of the solubility ($\log S$) were carried out using the stepwise strategy in the SPSS [44] (for Windows, 9.0) software. The WNN and ANN algorithms were written in MATLAB 6.1 [45] (Math Works) by the authors.

3.3. Descriptor selection

The selection of relevant descriptors, which relate the solubility to the molecular structure, is an important step to construct a predictive model. In this work, the stepwise multiple linear regression was used as the feature selection method to select the best calculated descriptors among 1481 theoretical descriptors using Dragon software. Those descriptors are divided into 18 different classes. The following method was used to select the most feasible descriptors using the training set:

- (1) All descriptors with zero values for all the molecules in the training set were eliminated. Two classes of the descriptors were the same for the anthraquinone dyes, therefore they were eliminated.

Table 2

Molecular descriptor classes in Dragon software and number of selected descriptors in each class at the primary step of descriptor selection

Molecular descriptor class	Number of descriptors in the class	Number of selected descriptors in the class	Adjusted squared correlation coefficient R^2
Constitutional descriptors	47	5	0.759
Topological descriptors	262	11	0.812
Molecular walk counts	21	1	0.563
BCUT descriptors	64	8	0.717
Galvez topological charge indices	21	10	0.808
2D autocorrelations	96	9	0.810
Charge descriptors	14	4	0.351
Aromaticity indices	4	2	0.228
Randic molecular profiles	41	1	0.171
Geometrical descriptors	58	8	0.726
RDF descriptors	150	8	0.772
3D-MoRSE descriptors	160	10	0.810
WHIM descriptors	99	11	0.812
GETAWAY descriptors	197	6	0.799
Functional groups	121	11	0.752
Atom-centered descriptors	120	9	0.753
Empirical descriptors	3	Non	–
Properties	3	Non	–

- (2) The variance–covariance matrix was calculated between the descriptors of each class and one of the two descriptors which has the pair wise correlation coefficient above 0.9 ($R > 0.9$) and it has a large correlation coefficient with the other descriptors was eliminated. The input variables in MLR must not be highly correlated.
- (3) MLR models were constructed with remaining descriptors of each class based on stepwise feature selection. The numbers of selected descriptors from each class and the adjusted squared correlation coefficient of the MLR models are in Table 2.
- (4) The selected descriptors from each class with the experimental descriptors, pressure and temperature, were used to select the best descriptors using stepwise MLR method. The result shows that six calculated and two experimental descriptors are the most feasible ones. The calculated descriptors are (1) number of nitrogen atom (nN), (2) maximum negative charge (qneg), (3) 1st component accessibility directional WHIM index/weighted by atomic masses (E1m), (4) V total size index/weighted by atomic electrotopological state (Vs), (5) Narumi geometrical topological index (GNar) and (6) mean information content on the distance degree equality (IDDE).

Although stepwise MLR model was used as a feature selection method, the final constructed MLR model was also used as a calibration model for predicting the solubility of anthraquinone dyes in SC-CO₂ conditions. The final MLR model with its coefficients and the mean effect of each selected descriptor are given in Table 3. The mean effect describes the influence of each descriptor on the MLR model. The predictive ability of the MLR model was evaluated by calculation of the RMSE and mean absolute error for the calibration and

Table 3
The coefficient and mean effect of descriptors in the MLR model

	Descriptor	Regression coefficient	Mean effect
1	Pressure	3.317×10^{-3}	0.750
2	Temperature	4.472×10^{-3}	1.507
3	Number of N atom	−0.617	−0.426
4	qneg	−12.116	−3.576
5	E1m	−3.059	−0.907
6	Vs	-2.46×10^{-3}	−0.193
7	GNar	−9.217	−19.00
8	IDDE	1.041	4.052
9	Constant	13.389	

prediction sets. The RMSE and mean absolute error were 0.324 and 0.247 for the prediction set and 0.388 and 0.277 for the validation data set.

3.4. Brief description of selected descriptors

The reason for selecting pressure and temperature as experimental descriptors is clear, it is well known that the density of the supercritical fluid is the key parameter to the solubility of different compounds and at the same time, the density is related to both temperature and pressure of the supercritical fluid. The comparison between mean effects of *T* and *P* shows that the effect of *T* on solubility are twice of the *P*. Topological descriptors (GNar [46] and IDDE) have the most effect on solubility. Weighted holistic invariant molecular descriptors (WHIM) (E1m and Vs) contain information about the whole molecular structure in terms of size, shape and

symmetry and atom distribution. These indices are calculated by a principal component analysis on Cartesian coordinates of the atoms weighted in four different ways. The used weights are the atomic masses, the van der Waals radii, the atomic electronegativities and the unitary weights [47–49]. Charge descriptor (qneg) has been reported previously [50]. According to classical chemical theory, all chemical interactions are by nature either electrostatic (polar) or orbital (covalent). Electrical charges in the molecule are obviously the driving force of electrostatic interactions. Indeed, it has been proven that local electron densities or charges are important in many chemical reactions and physiochemical properties of compounds. Thus charge based descriptors have been widely employed as chemical reactivity indices or as measures of weak intermolecular interactions. Many quantum-chemical descriptors are derived from the partial charge distribution in a molecule or from the electron densities on particular atoms. The number of nitrogen atom (nN) in the molecules as a constitutional descriptor is another relevant descriptor, which increases the correlation coefficient between the observed and the predicted solubility. The numerical values of the calculated descriptors for dyes are given in Table 4.

4. Results and discussion

4.1. Wavelet neural network model

WNN models were developed using eight nodes in input layer corresponding to the mentioned eight descriptors. The output layer had one node that predicts solubility. The number

Table 4
The calculated values of different descriptors by Dragon software, studied in this work

Dye	nN	qneg	E1m	Vs	GNar	IDDE
Blue 14	2	0.315	0.276	42.649	2.048	3.122
Red 11	0	0.291	0.294	27.732	2.053	3.572
Red 60	1	0.354	0.318	69.199	2.105	4.484
Blue 60	1	0.287	0.389	80.305	2.135	3.835
Blue 27	2	0.352	0.374	148.532	2.027	4.583
Blue 118	2	0.338	0.338	77.224	2.078	3.719
AQ1	0	0.285	0.256	23.445	2.091	3.735
AQ3	0	0.285	0.263	36.145	2.048	3.822
AQ5	0	0.285	0.327	53.535	2.043	4.152
AQ6	0	0.285	0.356	65.752	2.041	4.35
A2	0	0.284	0.265	41.41	2.045	4.107
A3	0	0.285	0.322	62.062	2.04	3.355
ACO3	2	0.279	0.208	77.105	2.04	3.585
ACO8	2	0.291	0.289	326.722	2.028	3.97
Quinizarin	0	0.329	0.259	27.236	2.053	3.17
Orange 11	1	0.38	0.252	26.493	2.053	3.572
1-Methylamino anthraquinone	1	0.312	0.28	31.012	2.086	3.614
Blue 3	2	0.32	0.275	64.365	2.043	4.096
Blue 77	2	0.352	0.303	93.987	2.051	4.209
AQ2	0	0.287	0.24	26.201	2.053	3.572
AQ4	0	0.285	0.284	43.497	2.045	3.69
AQ7	0	0.285	0.354	62.015	2.016	4.263
A1	0	0.284	0.257	26.342	2.053	3.086
A4	0	0.284	0.218	53.176	1.991	3.292
Blue 134	2	0.313	0.249	78.841	1.991	3.418

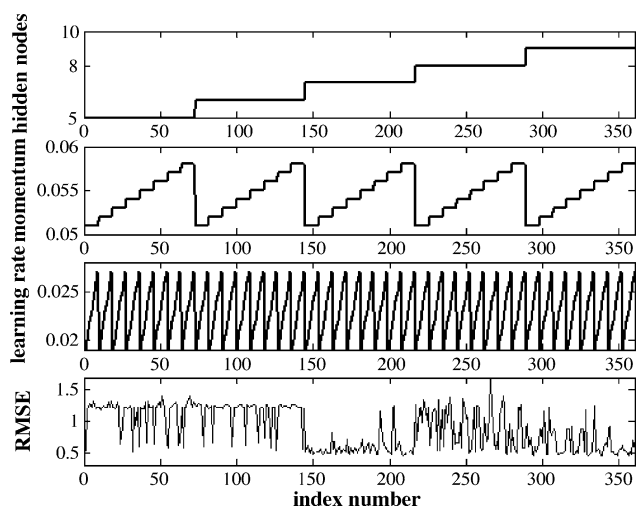


Fig. 2. Plots of (a) the number of nodes in the hidden layer against index number; (b) the momentum values; (c) the learning rate values; (d) the RMSE for the prediction set.

of nodes in the hidden layer is unknown and need to be optimized. In addition to the number of nodes in the hidden layer, the learning rate, the momentum and the number of iterations should also be optimized. In this work, the number of nodes in hidden layer and other parameters except the number of iterations were optimized simultaneously. In other words, the best value for each variable was not obtained by “one at a time” optimization method. The number of nodes in hidden layer can be changed from 2 to 11, while the learning rate from 0.001 to 0.1 with a step of 0.001 and momentum from 0.1 to 0.99 with a step of 0.01. The WNN models were constructed with all of the possible combinations of those three variables. The root mean square error (RMSE) for training and prediction sets for each WNN model was calculated. The WNN model, which shows minimum RMSE for training and prediction sets, was selected as the optimized WNN model and the variables of this model were selected as the optimized variable values. It was realized that the RMSE errors for the training and prediction sets are minimum when seven nodes were selected in the hidden layer and the learning rate and the momentum values were 0.023 and 0.54, respectively. Fig. 2 shows the changes of the variables values against the index number. Each number of index number corresponds to a combination of variable values and total number of index number is equal to the all possible combination of the variable values. In Fig. 2 only a subset of index numbers (350 of possible variable combinations) are shown. Fig. 2 comprises of plots showing the changes of (a) number of nodes in the hidden layer from 5 to 10 (b) the momentum values from 0.05 to 0.06 and (c) the learning rate from 0.020 to 0.027. Fig. 2d shows the RMSE for prediction set for each number of index numbers. Finally, the number of iterations was optimized with the optimized variable values. It was realized that at 6000 iterations, the RMSE errors for prediction set was minimum. The performance of the model was evaluated by plotting the estimated values versus experimental values of the solubility for the prediction and validation set (Fig. 3A and B). The RMSE and mean absolute

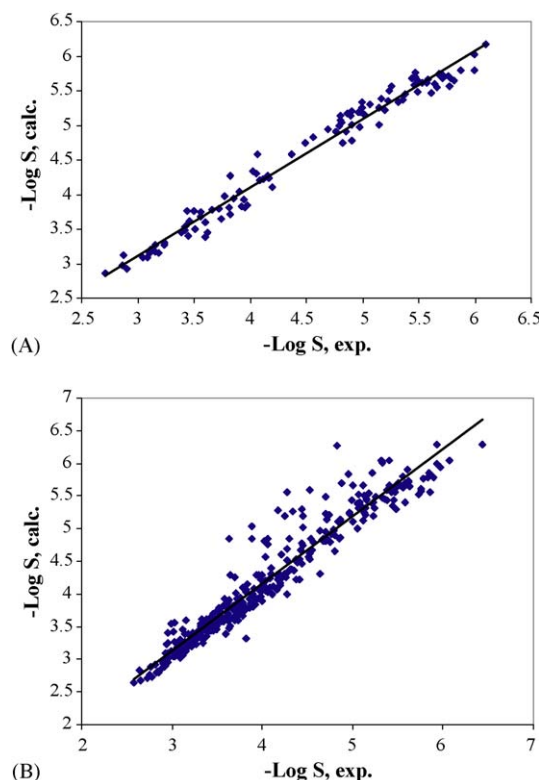


Fig. 3. Scatter plot of the calculated $\log(S)$ from WNN model against the experimental $\log(S)$ for the (A) prediction set ($R^2 = 0.973$) and (B) validation set ($R^2 = 0.926$).

errors were 0.271 and 0.190 for the prediction set and 0.339 and 0.221 for the validation set. Some of the results of the prediction ability of the model for validation set are given in Table 5. However, the ability of the model for all of the validation set is shown in Fig. 3B.

4.2. Artificial neural network model

In order to compare the predictive ability of WNN with another nonlinear model, a similar study was carried out using ANN model. A neural network was constructed with a sigmoid function as a hidden transfer function and linear function as output transfer function. A back propagation learning algorithm was employed to adjust the weights. ANN models were developed using eight nodes in input layer corresponding to the mentioned eight descriptors. The output layer had one node that predicts solubility. The number of nodes in the hidden layer is unknown and need to be optimized. In addition to the number of nodes in the hidden layer, the learning rate, the momentum and the number of iterations should also be optimized. The ANN architecture and its parameters were optimized simultaneously with the same procedure as was described for WNN. It was realized that the RMSE errors for the training and prediction sets are minimum when seven nodes were selected in the hidden layer and the learning rate and the momentum values were 0.032 and 0.76, respectively. The number of iteration was optimized after the optimization of the variables and it was realized that at 8000 iterations, the RMSE errors for prediction

Table 5
Experimental and calculated values of log(S) using ANN and WNN models for the validation set

Dye	P (bar)	T (K)	Experimental log(S) (mol/mol)	Calculated (ANN) log(S) (mol/mol)	Absolute error (ANN)	Calculated (WNN) log(S) (mol/mol)	Absolute error (WNN)
Blue 14	200	313.15	−5.873	−5.872	0.001	−5.814	0.059
Red 60	120	313.15	−5.484	−5.526	−0.042	−5.623	−0.139
	283.1	333.15	−4.75	−4.633	0.117	−4.793	−0.043
	181.1	363.15	−5.228	−5.294	−0.066	−5.203	0.025
Blue 60	243.9	333.15	−5.558	−5.588	−0.03	−5.804	−0.246
	252.5	363.15	−5.476	−5.386	0.09	−5.299	0.177
	282.4	393.15	−5.117	−5.066	0.051	−5.126	−0.009
	167	423.15	−5.436	−5.465	−0.029	−5.349	0.087
	224	393.15	−5.472	−5.391	0.081	−5.562	−0.09
Blue 27	200	373.15	−6.78	−5.567	1.213	−5.705	1.075
Blue 118	200	323.15	−6.076	−6.654	−0.578	−6.053	0.023
AQ1	182	308	−3.987	−3.847	0.14	−4.222	−0.235
	182	318	−4.022	−3.851	0.171	−4.126	−0.104
	334	318	−3.788	−3.682	0.106	−3.822	−0.034
	182	338	−3.896	−3.853	0.043	−4	−0.104
	334	338	−3.482	−3.345	0.137	−3.495	−0.013
AQ3	182	308	−3.78	−3.732	0.048	−3.796	−0.016
	274	328	−3.536	−3.781	−0.245	−3.643	−0.107
	182	348	−3.863	−3.816	0.047	−3.595	0.268
	274	348	−3.36	−3.351	0.009	−3.112	0.248
	243	318	−3.652	−3.564	0.088	−3.505	0.147
	334	318	−3.59	−3.529	0.061	−3.389	0.201
AQ5	243	308	−3.492	−3.514	−0.022	−3.46	0.032
	334	308	−3.366	−3.467	−0.101	−3.338	0.028
	182	348	−3.627	−3.775	−0.148	−3.599	0.028
	274	348	−3.012	−3.25	−0.238	−3.033	−0.021
	243	318	−3.283	−3.503	−0.22	−3.351	−0.068
	334	318	−3.149	−3.387	−0.238	−3.186	−0.037
	152	338	−3.782	−3.957	−0.175	−3.806	−0.024
	243	338	−3.17	−3.452	−0.282	−3.212	−0.042
AQ6	182	308	−3.392	−3.535	−0.143	−3.6	−0.208
	243	308	−3.283	−3.349	−0.066	−3.367	−0.084
	243	328	−3.186	−3.289	−0.103	−3.2	−0.014
	334	328	−2.909	−3.031	−0.122	−2.96	−0.051
	182	348	−3.551	−3.542	0.009	−3.58	−0.029
	274	338	−2.963	−3.102	−0.139	−3.02	−0.057
A2	202.6	308.15	−3.328	−3.336	−0.008	−3.419	−0.091
	202.6	328.15	−3.168	−3.316	−0.148	−3.244	−0.076
	364.8	338.15	−2.644	−2.637	0.007	−2.837	−0.193
A3	202.6	318.15	−4.347	−4.155	0.192	−4.365	−0.018
	243.2	328.15	−4.041	−3.954	0.087	−4.108	−0.067
	324.2	338.15	−3.692	−3.656	0.036	−3.743	−0.051
	324.2	328.15	−3.996	−3.951	0.045	−3.884	0.112
ACO3	90	305	−5.375	−5.407	−0.032	−5.587	−0.212
	135	330	−5.235	−5.417	−0.182	−5.309	−0.074
	150	340	−5.137	−5.331	−0.194	−5.21	−0.073
ACO8	123	296	−5.627	−5.687	−0.06	−5.642	−0.015
	670	291	−5.451	−5.565	−0.114	−5.44	0.011
	87	303.2	−5.827	−5.868	−0.041	−5.782	0.045
	126	324.7	−5.568	−5.646	−0.078	−5.671	−0.103
Quinizarine	270	353.15	−4.101	−3.965	0.136	−4.399	−0.298
	220	373.15	−4.216	−4.295	−0.079	−4.598	−0.382
	180	393.15	−4.677	−4.831	−0.154	−4.84	−0.163
Orange 11	100	313.15	−5.971	−7.672	−1.701	−5.945	0.026
	150	313.15	−5.497	−6.98	−1.483	−5.658	−0.161
	200	313.15	−5.154	−6.349	−1.195	−5.456	−0.302
	250	313.15	−5.086	−5.753	−0.667	−5.343	−0.257
1-Methylaminoanthraquinone	100	313.15	−5.78	−7.166	−1.386	−5.773	0.007
	200	313.15	−4.996	−5.886	−0.89	−5.103	−0.107
	250	313.15	−4.807	−5.351	−0.544	−4.892	−0.085
	100	393.15	−5.552	−8.32	−2.768	−5.628	−0.076
Blue 3	261.7	323.7	−4.802	−4.101	0.701	−4.662	0.14
	275.9	353.7	−4.522	−3.532	0.99	−4.533	−0.011

Table 5 (Continued)

Dye	P (bar)	T (K)	Experimental log(S) (mol/mol)	Calculated (ANN) log(S) (mol/mol)	Absolute error (ANN)	Calculated (WNN) log(S) (mol/mol)	Absolute error (WNN)
Blue 77	187.2	413.7	−4.865	−4.768	0.097	−4.864	0.001
	329.8	413.7	−4.197	−3.735	0.462	−4.22	−0.023
	300	373.15	−4.059	−4.195	−0.136	−4.758	−0.699
	400	373.15	−3.644	−5.038	−1.394	−4.288	−0.644
AQ2	122	308	−4.201	−4.213	−0.012	−4.293	−0.092
	182	328	−3.866	−3.926	−0.06	−3.859	0.007
	243	348	−3.438	−3.557	−0.119	−3.436	0.002
	213	338	−3.636	−3.756	−0.12	−3.641	−0.005
AQ4	182	338	−3.807	−3.948	−0.141	−3.807	0
	243	338	−3.495	−3.599	−0.104	−3.516	−0.021
	122	318	−4.229	−4.273	−0.044	−4.251	−0.022
	182	348	−3.757	−4.072	−0.315	−3.832	−0.075
	243	348	−3.417	−3.795	−0.378	−3.444	−0.027
	152	338	−4.032	−4.207	−0.175	−4.056	−0.024
	182	338	−3.767	−4.042	−0.275	−3.84	−0.073
	274	338	−3.309	−3.769	−0.46	−3.388	−0.079
	304	338	−3.235	−3.76	−0.525	−3.308	−0.073
	243	308	−3.582	−3.852	−0.27	−3.832	−0.25
	304	328	−3.288	−3.837	−0.549	−3.439	−0.151
	304	308	−3.075	−3.191	−0.116	−3.086	−0.011
AQ7	334	308	−3.068	−3.101	−0.033	−3.062	0.006
	243	328	−3.045	−3.358	−0.313	−3.068	−0.023
	274	328	−2.951	−3.171	−0.22	−2.95	0.001
	304	348	−2.754	−2.678	0.076	−2.765	−0.011
	334	348	−2.655	−2.411	0.244	−2.676	−0.021
	355	318	−2.915	−2.901	0.014	−2.918	−0.003
	213	338	−3.225	−3.522	−0.297	−3.223	0.002
	243.2	318.15	−4.26	−4.207	0.053	−4.252	0.008
A1	121.6	348.15	−4.854	−5.152	−0.298	−4.845	0.009
	283.7	338.15	−3.928	−3.913	0.015	−3.9	0.028
	364.8	318.15	−4.081	−4.117	−0.036	−4.097	−0.016
	324.2	318.15	−4.125	−4.108	0.017	−4.127	−0.002
	324.2	308.15	−4.252	−4.242	0.01	−4.295	−0.043
	324.2	328.15	−3.987	−3.964	0.023	−3.965	0.022
	364.8	328.15	−3.951	−3.935	0.016	−3.925	0.026
	121.6	308.15	−4.097	−3.667	0.43	−4.02	0.077
A4	162.1	308.15	−3.921	−3.508	0.413	−3.845	0.076
	243.2	318.15	−3.319	−3.307	0.012	−3.511	−0.192
	202.6	318.15	−3.62	−3.398	0.222	−3.606	0.014
	162.1	328.15	−3.745	−3.556	0.189	−3.691	0.054
	202.6	328.15	−3.42	−3.4	0.02	−3.506	−0.086
Blue 134	100	323.15	−5.931	−5.387	0.544	−5.988	−0.057
	120	353.15	−5.84	−5.671	0.169	−5.855	−0.015

set was minimum. The RMSE and mean absolute errors were 0.177 and 0.131 for the prediction set and 0.463 and 0.287 for the validation set. Some of the results for the validation set are given in Table 5.

5. Conclusions

The WNN model was developed for predicting the solubility for 25 anthraquinone dyes in supercritical carbon dioxide over a wide range of pressure (70–770 bar) and temperature (291–423 K). The performance of the WNN model was compared with MLR and ANN models. The results indicate the superiority of the WNN model over that of the other models.

Acknowledgements

Thanks were given to Prof. Todeschini and other members in Milano Chemometrics and QSPR Research Group for providing the Dragon package, used in this research. The authors acknowledge to the Research Council of Isfahan University of Technology and Center of Excellency in Chemistry of Isfahan University of Technology for the support of this work.

References

- [1] B. Gebert, W. Saus, D. Knittel, H.J. Bushman, E. Schollmeyer, Text. Res. J. 64 (1994) 371.
- [2] W. Knittel, E. Schollmeyer, Melliand Textilber 76 (1995) 1092.

- [3] E. Bach, E. Cleve, E. Scholleyer, Dyeing of poly(ethylene terephthalate) fibers in supercritical carbon dioxide, in: Ph.R. von Rohr, Ch. Trepp (Eds.), *High-Pressure Chemical Engineering*, Elsevier Science, Amsterdam, 1996, pp. 581–586.
- [4] K.H. Chang, H.K. Bae, J.J. Shim, Korean J. Chem. Eng. 13 (1996) 310.
- [5] W. Saus, D. Knittel, E. Schollmeyer, Text. Res. J. 63 (1993) 135.
- [6] S.N. Joung, K.P. Yoo, J. Chem. Eng. Data 43 (1998) 9.
- [7] B. Guzel, A. Akgerman, J. Chem. Eng. Data 44 (1999) 83.
- [8] H.D. Sung, J.J. Shim, J. Chem. Eng. Data 44 (1999) 985.
- [9] J.W. Lee, J.M. Min, H.K. Bae, J. Chem. Eng. Data 44 (1999) 684.
- [10] J.W. Lee, M.W. Park, H.K. Bae, Fluid Phase Equilib. 179 (2001) 387.
- [11] K. Tamura, T. Shinoda, Fluid Phase Equilib. 219 (2004) 25.
- [12] S.L. Draper, G.A. Montero, B. Smith, K. Beck, Dyes and Pigments 45 (2000) 177.
- [13] K. Mishima, K. Matsuyama, H. Ishikawa, K. Hayashi, S. Maeda, Fluid Phase Equilib. 194–197 (2002) 895.
- [14] M. Shamsipur, A.R. Karami, Y. Yamini, H. Sharghi, J. Supercrit. Fluids 32 (2004) 47.
- [15] M.R. Fat'hi, Y. Yamini, H. Sharghi, M. Shamsipur, Talanta 48 (1999) 951.
- [16] A. Ferri, M. Banchero, L. Manna, S. Sicardi, J. Supercrit. Fluids 30 (2004) 41.
- [17] D. Tuma, G.M. Schneider, Fluid Phase Equilib. 158–160 (1999) 743.
- [18] C.B. Kautz, B. Wagner, G.M. Schneider, J. Supercrit. Fluids 13 (1998) 43.
- [19] D. Tuma, B. Wagner, G.M. Schneider, Fluid Phase Equilib. 182 (2001) 133.
- [20] B. Wagner, C.B. Kautz, G.M. Schneider, Fluid Phase Equilib. 158–160 (1999) 707.
- [21] D. Tuma, G.H. Schneider, J. Supercrit. Fluids 13 (1998) 37.
- [22] T. Kraska, K.O. Leonhard, D. Tuma, G.M. Schneider, Fluid Phase Equilib. 194–197 (2002) 469.
- [23] J. Chrastil, J. Phys. Chem. 86 (1982) 3016.
- [24] J. Mendez-Santiago, A.S. Teja, Fluid Phase Equilib. 158–160 (1999) 501.
- [25] J.M. Del Valle, J.M. Aguilera, Ind. Eng. Chem. Res. 27 (1998) 1551.
- [26] M.D. Gordillo, M.A. Blanco, A. Molero, E. Martinez de la Ossa, J. Supercrit. Fluids 15 (1999) 183.
- [27] A. Jouyban, H. Chan, N.R. Foster, J. Supercrit. Fluids 24 (2002) 19.
- [28] A. Ferri, M. Banchero, L. Manna, S. Sicardi, J. Supercrit. Fluids 32 (2004) 27.
- [29] D.Y. Peng, D.B. Robinson, Ind. Eng. Chem. Fundam. 15 (1976) 59.
- [30] P. Politzer, J.S. Murray, P. Lane, T. Brink, J. Phys. Chem. 97 (1993) 729.
- [31] P. Politzer, P. Lane, J.S. Murray, T. Brink, J. Phys. Chem. 96 (1992) 7938.
- [32] Z. Huang, S. Kawi, Y.C. Chiew, Fluid Phase Equilib. 216 (2004) 111.
- [33] P. Battersby, J.R. Dean, W.R. Tomlinson, S.M. Hitchen, P. Myers, Analyst 119 (1994) 925.
- [34] T. Khayamian, M. Esteki, J. Supercrit. Fluids 32 (2004) 73.
- [35] A.K. Leung, F. Chau, J. Gao, Chemom. Intell. Lab. Syst. 43 (1998) 165.
- [36] I. Daubechies (Ed.), *Ten Lectures on Wavelets*, SIAM Press, Philadelphia, 1992.
- [37] B. Walczak, *Wavelets in Chemistry*, Elsevier Science, Amsterdam, 2000.
- [38] Q. Guo, L. Liu, W. Cai, Y. Liu, Chem. Phys. Lett. 514 (1998) 518.
- [39] L. Liu, Q. Guo, J. Chem. Inf. Comput. Sci. 39 (1999) 133.
- [40] X. Zhang, J. Qi, R. Zhang, M. Liu, Z. Hu, H. Xue, B. Fan, Comput. Chem. 25 (2001) 125.
- [41] T. Khayamian, A.A. Ansafi, R. Tabaraki, M. Esteki, Anal. Lett. 38 (2005) 1477.
- [42] Hyperchem.6.Hypercube, Inc., 2000.
- [43] R. Todeschini, Milano Chemometrics and QSPR Group. <http://www.di-sat.unimib.it/vhml/>.
- [44] SPSS for windows, Statistical Package for IBM PC, SPSS Inc., 1993. <http://WWW.SPSS.com>.
- [45] MATLAB 6.1, The Math Works, Inc., Natick, MA.
- [46] H. Narumi, MATCH Comm. Math. Comp. Chem. J. 22 (1987) 195–207.
- [47] R. Todeschini, M. Lasagni, E. Marengo, J. Chemom. 8 (1994) 263.
- [48] R. Todeschini, P. Gramatica, R. Provenzani, E. Marengo, Chemom. Intell. Lab. Syst. 27 (1995) 221.
- [49] P. Gramatica, N. Navas, R. Todeschini, Chemom. Intell. Lab. Syst. 40 (1998) 53.
- [50] M. Karelson, V.S. Lobanov, A.R. Katritzky, Chem. Rev. 96 (1996) 1027.